

High-precision abundances of elements in *Kepler* LEGACY stars

Verification of trends with stellar age [★], ^{★★}

P. E. Nissen, V. Silva Aguirre, J. Christensen-Dalsgaard, R. Collet, F. Grundahl, and D. Slumstrup

Stellar Astrophysics Centre, Department of Physics and Astronomy, Aarhus University, Ny Munkegade 120, DK-8000 Aarhus C, Denmark. e-mail: pen@phys.au.dk.

Received 28 August 2017/ Accepted 29 September 2017

ABSTRACT

Context. A previous study of solar twin stars has revealed the existence of correlations between some abundance ratios and stellar age providing new knowledge about nucleosynthesis and Galactic chemical evolution.

Aims. High-precision abundances of elements are determined for stars with asteroseismic ages in order to test the solar twin relations.

Methods. HARPS-N spectra with signal-to-noise ratios $S/N \gtrsim 250$ and MARCS model atmospheres were used to derive abundances of C, O, Na, Mg, Al, Si, Ca, Ti, Cr, Fe, Ni, Zn, and Y in ten stars from the *Kepler* LEGACY sample (including the binary pair 16 Cyg A and B) selected to have metallicities in the range $-0.15 < [\text{Fe}/\text{H}] < +0.15$ and ages between 1 and 7 Gyr. Stellar gravities were obtained from seismic data and effective temperatures were determined by comparing non-LTE iron abundances derived from Fe I and Fe II lines. Available non-LTE corrections were also applied when deriving abundances of the other elements.

Results. The abundances of the *Kepler* stars support the $[\text{X}/\text{Fe}]$ -age relations previously found for solar twins. $[\text{Mg}/\text{Fe}]$, $[\text{Al}/\text{Fe}]$, and $[\text{Zn}/\text{Fe}]$ decrease by ~ 0.1 dex over the lifetime of the Galactic thin disk due to delayed contribution of iron from Type Ia supernovae relative to prompt production of Mg, Al, and Zn in Type II supernovae. $[\text{Y}/\text{Mg}]$ and $[\text{Y}/\text{Al}]$, on the other hand, increase by ~ 0.3 dex, which can be explained by an increasing contribution of *s*-process elements from low-mass AGB stars as time goes on. The trends of $[\text{C}/\text{Fe}]$ and $[\text{O}/\text{Fe}]$ are more complicated due to variations of the ratio between refractory and volatile elements among stars of similar age. Two stars with about the same age as the Sun show very different trends of $[\text{X}/\text{H}]$ as a function of elemental condensation temperature T_c and for 16 Cyg, the two components have an abundance difference, which increases with T_c . These anomalies may be connected to planet-star interactions.

Key words. Stars: abundances – Stars: fundamental parameters – Stars: oscillations – Planet-star interactions – Galaxy: disk – Galaxy: evolution

1. Introduction

Precise determinations of abundances of elements in solar twin stars have revealed significant variations of some abundance ratios, for example $[\text{Mg}/\text{Fe}]$ and $[\text{Y}/\text{Mg}]$, tightly correlated with stellar age (Nissen 2015, 2016; Spina et al. 2016a,b; Tucci Maia et al. 2016; Adibekyan et al. 2016, 2017). This is of high interest for studies of nucleosynthesis and chemical evolution in our Galaxy. As the ages of the solar twins were derived from isochrones in the $T_{\text{eff}} - \log g$ plane and thus depend on the spectroscopically determined values of effective temperature and surface gravity, there is, however, a need to test the correlations using stellar ages determined in an independent way.

Asteroseismology provides an alternative method to determine reliable stellar ages. By fitting oscillation frequencies including the large and small frequency separations (Christensen-Dalsgaard 1988) by stellar models, ages can be obtained (see review by Christensen-Dalsgaard 2016). Thus, Silva Aguirre et al. (2015) derived ages of 33 exoplanet host stars from oscillation frequencies delivered by the *Kepler* mission. More recently, Lund et al. (2017) have measured precise

oscillation frequencies for 66 main-sequence and subgiant stars for which long *Kepler* time series are available. The data for this so-called *Kepler* LEGACY sample have been analysed in Silva Aguirre et al. (2017) by seven teams using different stellar models and methods to fit the frequencies. Constraints on effective temperature, T_{eff} , and metallicity, $[\text{Fe}/\text{H}]$, were adopted from an analysis of high-resolution spectra with signal-to-noise (S/N) ratios of about 30 by Buchhave & Latham (2015). The resulting seismic ages were estimated to have uncertainties of typically 10% - 20%. Furthermore, stellar masses and radii were determined with uncertainties at a level of 2% - 4%, and surface gravities, $\log g$, with errors less than 0.01 dex.

In this paper we have derived precise abundances for a subset of the *Kepler* LEGACY stars by analysing high-resolution HARPS-N spectra with $S/N \gtrsim 250$ and have investigated if the relations between various abundance ratios and stellar age obtained for solar twins are confirmed. Based on the Buchhave & Latham (2015) data, the stars were selected to have T_{eff} between 5700 K and 6400 K and $[\text{Fe}/\text{H}]$ between -0.15 and $+0.15$. The metallicity range is similar to that of the solar twins ($-0.10 < [\text{Fe}/\text{H}] < +0.10$), but the range in effective temperature is much larger. For the solar twins, an age range of about 9 Gyr arises because of differences in surface gravity, whereas the age range (1 - 7 Gyr) of the selected LEGACY stars is primarily due to differences in T_{eff} .

* Based on spectra obtained with HARPS-N@TNG under programme A33TAC_1.

** Tables 1 and 2 are also available in electronic form at the CDS via anonymous ftp to cdsarc.u-strasbg.fr (130.79.128.5) or via <http://cdsweb.u-strasbg.fr/cgi-bin/qcat?J/A+A/>

The paper is structured as follows: In Section 2, we describe the observations and reduction of the HARPS-N spectra. In Section 3, we are dealing with the determination of T_{eff} and abundances of elements including a discussion of non-LTE corrections. Section 4 is devoted to a discussion of the trends of various abundance ratios as a function of stellar age and a detailed discussion of the binary pair, 16 Cyg A and B. Finally, in Section 5 we present a concluding summary.

2. Observations and data reductions

The spectroscopic observations of the *Kepler* LEGACY stars were carried out July 19 - 22, 2016 with the HARPS-N spectrograph (Cosentino et al. 2012) at the 3.6 m Telescopio Nazionale Galileo (TNG) on La Palma. HARPS-N is an updated version of the HARPS-S instrument at the ESO 3.6 m telescope on La Silla, which was used to obtain spectra of the solar twins analysed in Nissen (2015, hereafter Paper I). The two spectrographs cover the wavelength range from 3800 Å to 6900 Å with a resolution of $R = \lambda/\Delta\lambda \sim 115\,000$ and a sampling of 3.3 pixels per spectral resolution element.

Extraction of spectra, flat fielding and wavelength calibration were done on-line with the HARPS-N data reduction pipeline. Individual spectra for a given star were combined in IRAF after correction for Doppler shifts and normalized to a continuum level of ~ 1.0 as described in Paper I. Furthermore, the IRAF `splot` task was used to measure equivalent widths of the spectral lines listed in Table 2 of Paper I by Gaussian fitting to the line profiles relative to continuum regions lying within 3 Å from the line measured.

Due to poor seeing and dust in the atmosphere only about half of the planned programme was completed, but for 12 stars spectra with $S/N \gtrsim 250$ were obtained. The quality of the spectra is illustrated in Fig. 1, which shows some typical lines used to determine abundances. As seen the ratio of the strengths of the Fe II and the Fe I lines increases very significantly with T_{eff} over the range covered. The ratio also depends on $\log g$, but since this parameter is precisely known from the seismic data, the equivalent widths of Fe II lines relative to those of Fe I become a sensitive measure of T_{eff} .

As seen from Fig. 1, two stars turn out to be double-lined spectroscopic binaries. For KIC 9025370, two sets of well separated lines are present and for KIC 10454113, the secondary component disturbs the right wings of the lines of the primary component. These two stars were excluded from the abundance analysis. Secondary oscillation spectra were not detected by Lund et al. (2017), but as discussed by Silva Aguirre et al. (2017) asteroseismic distances of these stars disagree with Gaia DR1 parallaxes (Gaia Collaboration et al. 2016a,b).

As described in Sect. 3, stellar abundances were derived by performing a differential analysis relative to the Sun. It is therefore important to have available a solar flux spectrum observed with the same spectrograph as the stars (Bedell et al. 2014). We were not able to observe such a spectrum with HARPS-N and used instead the HARPS-S spectrum of reflected sunlight from the asteroid Vesta that was also used in Paper I to derive abundances of solar twins. This solar flux spectrum has a very high S/N of 1200. As the two instruments are almost identical, no offset between the two sets of abundances is expected, but as a check the bright solar twin, 18 Sco (HD 146233), that were included in Paper I and have a HARPS-S spectrum with $S/N = 850$ was observed with HARPS-N with a similar high S/N . Equivalent widths measured in the two spectra for 132

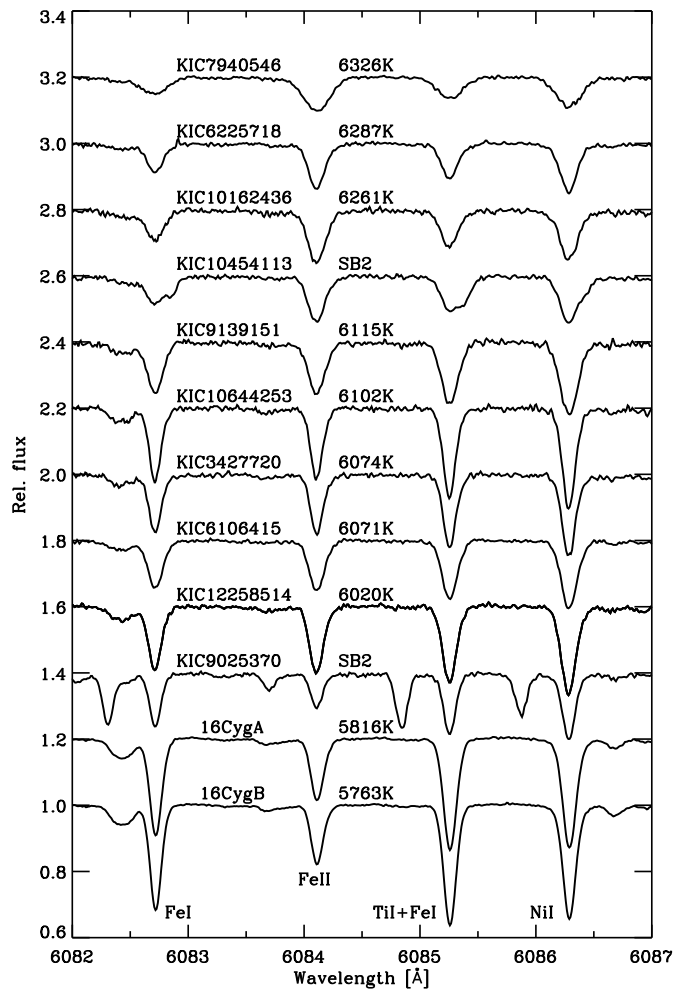


Fig. 1. HARPS-N spectra in the 6082 Å - 6087 Å region arranged in order of increasing T_{eff} and offset in successive steps of 0.2 units relative to the spectrum of 16 Cyg B. The spectra are marked with the T_{eff} values determined in this paper except for the two spectroscopic binaries.

spectral lines agree very well, that is with an average deviation of $\langle \Delta(N-S) \rangle = 0.1 \text{ mÅ}$ and a standard deviation of $\pm 0.5 \text{ mÅ}$. Furthermore, the derived abundances of 14 elements agree with $\langle \Delta(N-S) \rangle = 0.001 \pm 0.006 \text{ dex}$. This shows that the abundances in this paper are on the same system as that of the solar twins in Paper I.

3. Analysis

The Uppsala EQWIDTH program together with 1D MARCS models (Gustafsson et al. 2008) were used to determine elemental abundances from the measured equivalent widths assuming local thermodynamic equilibrium (LTE). The analysis was made differentially line-by-line to the Sun; hence, the oscillator strengths of the lines cancel out. Doppler broadening due to microturbulence was specified with a parameter ξ_{turb} added in quadrature to the thermal broadening. Further details including references for collisional broadening may be found in Paper I.

The spectral lines are also broadened by macroturbulence and stellar rotation, but this does not change the equivalent width of the lines, so in principle there is no effect on the derived abundances. Rapid rotation makes it, however, more difficult to measure precise values of equivalent widths due to broader lines

and more line blending. It is not a great problem for our set of stars, for which the projected equatorial velocity, $V \sin i$, ranges from 1.4 km s^{-1} to about 10 km s^{-1} (see Table 1), although some of the lines listed in Table 2 of Paper I had to be excluded for the warmest and most rapidly rotating stars due to line blending problems.

3.1. Atmospheric parameters

For the surface gravity, we adopted the mean of the seven seismic $\log g$ values derived in Silva Aguirre et al. (2017). An effective temperature, $T_{\text{eff}}(\text{ion})$, was then determined so that the Fe abundance determined from Fe I lines, $[\text{Fe}/\text{H}]_{\text{I}}$, is the same as the Fe abundance determined from Fe II lines, $[\text{Fe}/\text{H}]_{\text{II}}$. Furthermore, an effective temperature, $T_{\text{eff}}(\text{exc})$, was determined by requesting that the slope of $[\text{Fe}/\text{H}]$ vs. excitation potential for Fe I lines should be zero.

As the derived Fe abundances depend on the microturbulence, this parameter has to be determined together with $T_{\text{eff}}(\text{ion})$ and $T_{\text{eff}}(\text{exc})$ from the requirement that the slope of $[\text{Fe}/\text{H}]$ versus equivalent width is zero. In addition, one must ensure that the parameters of the MARCS model applied are consistent with those derived. Hence, the determination of T_{eff} , $[\text{Fe}/\text{H}]$, and ξ_{turb} is an iterative process.

In deriving the atmospheric parameters, non-LTE corrections from Lind et al. (2012) were taken into account. $[\text{Fe}/\text{H}]_{\text{II}}$ is not significantly affected but the non-LTE correction of $[\text{Fe}/\text{H}]_{\text{I}}$ increases from being negligible for 16 Cyg A and B to about $+0.02$ dex for stars with T_{eff} around 6300 K and $\log g \sim 4.0$. The corresponding change of $T_{\text{eff}}(\text{ion})$ is about -30 K, whereas the change of $T_{\text{eff}}(\text{exc})$ is about $+10$ K.

In the statistical-equilibrium calculations for iron by Lind et al. (2012), the classical formula (Drawin 1969; Steenbock & Holweger 1984) for the cross section of collisions with hydrogen atoms was adopted without any scaling factor. Recently, Amarsi et al. (2016b) have made new non-LTE calculations for iron using quantum-mechanical cross sections for excitation and ionization due to collisions with hydrogen atoms. Applying these corrections for our set of stars, we find similar small non-LTE effects as those based on the Lind et al. (2012) calculations; the rms difference is 10 K in both $T_{\text{eff}}(\text{ion})$ and $T_{\text{eff}}(\text{exc})$, part of which may be due to numerical problems when interpolating in the grids of corrections. Hence, the new calculations do not change our results significantly and we prefer to keep the Lind et al. (2012) corrections, which change more smoothly as a function of T_{eff} , $\log g$, and $[\text{Fe}/\text{H}]$ than the Amarsi et al. (2016b) corrections.

The derived atmospheric parameters are given in Table 1. Taking into account correlations between the parameters, the errors have been calculated from the standard errors of the mean values of $[\text{Fe}/\text{H}]_{\text{I}}$ and $[\text{Fe}/\text{H}]_{\text{II}}$ (estimated from the line-to-line scatter), the errors of the slopes of $[\text{Fe}/\text{H}]$ versus excitation potential and equivalent width, and an estimated error of 0.01 dex for $\log g$. This small error of the seismic gravity is justified in Silva Aguirre et al. (2017); the uncertainties of the observed frequencies introduce an error of typically 0.005 dex in $\log g$, and a comparison of gravities determined by the seven analysis teams shows a rms deviation ranging from 0.002 dex to 0.010 dex for our set of stars.

In contrast to $T_{\text{eff}}(\text{ion})$, $T_{\text{eff}}(\text{exc})$ is not sensitive to the adopted value of the surface gravity, because the strengths of the Fe I lines used to determine the slope of $[\text{Fe}/\text{H}]$ versus excitation potential change very little with $\log g$. Therefore, a comparison of $T_{\text{eff}}(\text{ion})$ and $T_{\text{eff}}(\text{exc})$ provides a test of the claimed precision

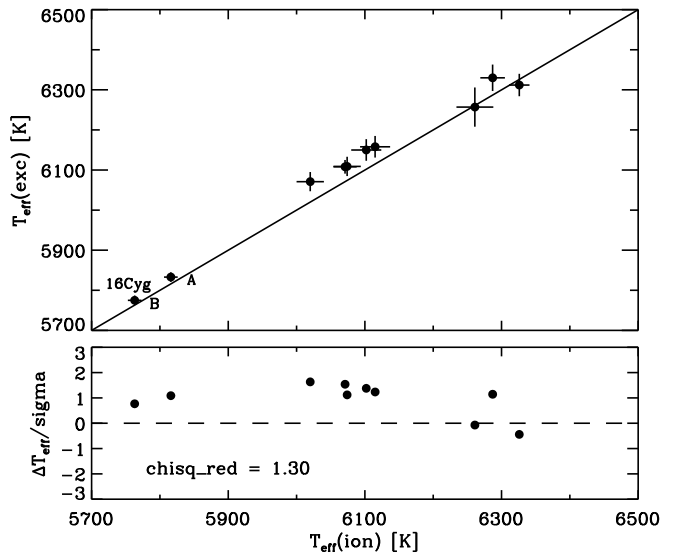


Fig. 2. $T_{\text{eff}}(\text{exc})$ versus $T_{\text{eff}}(\text{ion})$. The lower panel shows the difference $T_{\text{eff}}(\text{exc}) - T_{\text{eff}}(\text{ion})$ in units of the combined error: $\sigma = \sqrt{\sigma T_{\text{eff}}(\text{ion})^2 + \sigma T_{\text{eff}}(\text{exc})^2}$.

of the temperatures. As seen from Fig. 2, there is a satisfactory agreement in the sense that the deviations lie within about 1.8σ and have a reduced chi-square of $\chi_{\text{red}}^2 = 1.3$. There is, however, a puzzling systematic offset between $T_{\text{eff}}(\text{exc})$ and $T_{\text{eff}}(\text{ion})$ for 16 Cyg A and B ($\langle \Delta \rangle = 15$ K) and the five stars with T_{eff} around 6100 K ($\langle \Delta \rangle = 43$ K). It is unlikely that this is due to systematic errors in the non-LTE corrections, because for 16 Cyg A and B the corrections are insignificant.

The difference in $T_{\text{eff}}(\text{exc})$ and $T_{\text{eff}}(\text{ion})$ for 16 Cyg A and B disappears if the gravities are increased by approximately 0.03 dex. It is, however, very unlikely that such a systematic error is present in the seismic gravities. Using the Hipparcos parallaxes for 16 Cyg A and B, 47.44 ± 0.27 mas and 47.14 ± 0.27 mas, respectively (van Leeuwen 2007), to determine the luminosities and estimating masses by interpolation between ASTEC evolutionary tracks (Christensen-Dalsgaard 2008b) in the $L - T_{\text{eff}}$ diagram, the basic relations between gravity, mass, radius, luminosity, and effective temperature, $g \propto M/R^2$ and $R^2 \propto L/T_{\text{eff}}^4$, lead to $\log g = 4.285 \pm 0.010$ for 16 Cyg A and $\log g = 4.347 \pm 0.010$ for 16 Cyg B in good agreement with the seismic gravities.

A change in the helium abundance of the model atmospheres applied is another possibility to explain the discrepancy between $T_{\text{eff}}(\text{exc})$ and $T_{\text{eff}}(\text{ion})$. For late-type stars, helium does not contribute to opacity and free electrons, but it affects the mean molecular weight and hence the pressure in the atmosphere. As discussed by Böhm-Vitense (1979) and Strömgren et al. (1982), the effect on spectral lines of a change in He abundance is equivalent to a change in gravity given by Eq. (12) in Strömgren et al. (1982). The MARCS model atmospheres have been computed with a He abundance ratio of $N_{\text{He}}/N_{\text{H}} = 0.085$, which corresponds to a He mass fraction of $Y = 0.249$ close to the solar surface value of $Y = 0.24 - 0.25$ determined from helioseismology (e.g. Christensen-Dalsgaard & Pérez Hernández 1991; Vorontsov et al. 1991; Basu & Antia 2004). If instead, the He abundance in the atmospheres of 16 Cyg A and B is $Y \simeq 0.32$, the derived values of $T_{\text{eff}}(\text{exc})$ and $T_{\text{eff}}(\text{ion})$ would agree. There is, however, no evidence for enhanced He abundances in the atmospheres of 16 Cyg A and B. From the amplitude of a small oscillatory signature in the stellar oscillation frequencies caused

Table 1. List of stars with derived atmospheric parameters and seismic data.

KIC no.	ID	S/N ^a	$T_{\text{eff}}(\text{ion})$ [K]	$T_{\text{eff}}(\text{exc})$ [K]	[Fe/H] [dex]	ξ_{turb} km s ⁻¹	$\log g^b$ [dex]	Age ^b [Gyr]	$V\text{sini}^c$ km s ⁻¹
3427720	BD +38 3428	280	6074 ± 20	6109 ± 24	-0.024 ± 0.017	1.28 ± 0.06	4.386	2.4 ± 0.3	4.0
6106415	HD 177153	400	6071 ± 14	6108 ± 17	-0.037 ± 0.012	1.29 ± 0.04	4.299	4.8 ± 0.6	4.0
6225718	HD 187637	370	6287 ± 18	6330 ± 33	-0.110 ± 0.014	1.49 ± 0.06	4.319	2.6 ± 0.4	5.0
7940546	HD 175226	430	6326 ± 15	6312 ± 28	-0.126 ± 0.012	1.71 ± 0.05	4.005	2.4 ± 0.3	9.7
9139151	BD +45 2796	250	6115 ± 22	6158 ± 27	+0.096 ± 0.019	1.28 ± 0.06	4.379	1.9 ± 0.7	6.0
10162436	HD 188819	250	6261 ± 27	6257 ± 49	-0.073 ± 0.021	1.57 ± 0.09	3.977	2.5 ± 0.4	6.5
10644253	BD +48 2683	250	6102 ± 22	6150 ± 27	+0.130 ± 0.019	1.17 ± 0.06	4.403	1.3 ± 0.7	3.8
12069424	16 Cyg A	800	5816 ± 10	5833 ± 12	+0.093 ± 0.007	1.13 ± 0.02	4.291	7.0 ± 0.5	2.2
12069449	16 Cyg B	800	5763 ± 10	5775 ± 12	+0.062 ± 0.007	1.06 ± 0.02	4.356	7.1 ± 0.5	1.4
12258514	HD 183298	270	6020 ± 20	6071 ± 24	+0.027 ± 0.017	1.37 ± 0.06	4.124	4.5 ± 0.8	3.5

Notes. ^(a) Signal-to-noise ratio per spectral pixel at 6000 Å. ^(b) Seismic values of surface gravity and age from Silva Aguirre et al. (2017). ^(c) Projected equatorial rotation velocity; for 16 Cyg A and B seismic values from Davies et al. (2015) are given, whereas spectroscopic values from Bruntt et al. (2012) are given for the other stars.

by acoustic glitches in the helium ionization zone, Verma et al. (2014) found the surface He abundance of 16 Cyg A and B to lie in the range $0.22 \lesssim Y \lesssim 0.26$.

Hydrodynamical effects on the structure of stellar atmospheres is a third possibility to explain the systematic difference between $T_{\text{eff}}(\text{exc})$ and $T_{\text{eff}}(\text{ion})$. The MARCS models assume plane-parallel (1D) layers in hydrostatic equilibrium, whereas real atmospheres are better represented by 3D hydrodynamical models as shown by Lind et al. (2017) in a study of the centre-to-limb variation of Fe lines in the solar spectrum. A corresponding 3D non-LTE analysis of F and G stars is not available yet, but Amarsi et al. (2016b) have calculated grids of ⟨3D⟩ non-LTE corrections of Fe abundances derived from MARCS models, where ⟨3D⟩ refers to horizontally- and temporally-averaged 3D STAGGER model atmospheres (Magic et al. 2013). We have interpolated in these grids to find differential corrections for our set of Fe lines, but this does not improve the agreement between $T_{\text{eff}}(\text{exc})$ and $T_{\text{eff}}(\text{ion})$.

It remains to be seen if a more complete 3D non-LTE analysis will remove the systematic offset between $T_{\text{eff}}(\text{exc})$ and $T_{\text{eff}}(\text{ion})$. For the time being, we have to accept that there could be systematic errors in T_{eff} of the same order of size as the statistical errors quoted in Table 1. As the errors of $T_{\text{eff}}(\text{ion})$ are smaller than those of $T_{\text{eff}}(\text{exc})$, we shall adopt $T_{\text{eff}}(\text{ion})$ when deriving stellar abundances.

3.2. Abundances

In this section, we describe how the abundances of elements were derived and discuss non-LTE corrections and possible systematic errors. Statistical errors arising from the equivalent width measurements, σ_{EW} , are estimated from the line-to-line scatter of the derived abundances. For 16 Cyg A and B having spectra with $S/N \sim 800$ like the solar twins, σ_{EW} was adopted from Paper I (Table 4). For the other eight stars with $S/N \sim 250$ –400, we calculated an average standard deviation $\langle\sigma[X/H]\rangle$ (see Eqs. (2) and (3) in Nissen 2016) and then the standard error of the mean value of $[X/H]$ from the expression $\sigma_{\text{EW}} = \langle\sigma[X/H]\rangle / \sqrt{N_{\text{lines}}}$.

3.2.1. Non-LTE corrections and statistical errors

Carbon. The C abundances were derived from the two high-excitation ($\chi_{\text{exc}} = 7.69$ eV) C I lines at 5052.2 Å and 5380.3 Å. The equivalent widths of these lines range from 20 mÅ to 55 mÅ in our set of stars. According to Takeda & Honda (2005), who adopted the Drawin (1969) cross sections for collisions with hydrogen atoms, differential non-LTE corrections relative to the corrections for the Sun are getting more negative with increasing T_{eff} and decreasing gravity. The corrections are negligible for 16 Cyg A and B, but of some importance for the warmer stars, that is -0.02 dex for the 5052.2 Å line and -0.01 dex for the weaker 5380.3 Å line at $T_{\text{eff}} \sim 6300$ K and $\log g \sim 4.0$. After applying the non-LTE corrections, the C abundances derived from the two C I lines have an average standard deviation of $\langle\sigma[C/H]\rangle = 0.017$ dex for the eight stars with $T_{\text{eff}} > 6000$ K, corresponding to $\sigma_{\text{EW}}[C/H] = 0.012$ dex.

Oxygen. For solar twins, O abundances were derived from the [O I] 6300.3 Å line taking into account a correction of the measured equivalent width due to a Ni I blend (Allende Prieto et al. 2001). This [O I] line is very weak in our warmer stars; therefore, we have included the O I 6158.2 Å line, which is well separated from the nearby Fe I 6157.7 Å line in HARPS spectra. The equivalent width of this oxygen line increases from 3.6 mÅ in the solar flux spectrum to about 9 mÅ for the warmest star, KIC 7940546. As shown by Bertran de Lis et al. (2015), O abundances derived from the two oxygen lines agree well for a large set of solar-type stars with HARPS spectra.

Recently, Amarsi et al. (2016a) have studied non-LTE oxygen line formation across a grid of 3D hydrodynamic STAGGER model atmospheres and provided 3D non-LTE corrections of O abundances determined with MARCS models. In contrast to the case of the O I 777 nm triplet, the corrections for the 6158.2 Å and 6300.3 Å lines are small. Using the IDL interpolation program provided, the differential corrections of O abundances derived from the O I 6158.2 Å line are found to range from being negligible for 16 Cyg A and B to -0.03 dex as the most extreme value for our sample of stars. In the case of the [O I] 6300.3 Å line, the most extreme differential correction is only -0.01 dex. This small correction arises entirely from 3D effects, because LTE is a very good approximation for this forbidden line (e.g. Kiselman 1993).

The oxygen abundances derived from the two O I lines agree with an average standard deviation of $\langle\sigma[\text{O}/\text{H}]\rangle = 0.032$ dex. This is higher than in the case of carbon, which is due to larger relative errors for the equivalent widths of the weak oxygen lines. For one star, KIC 10162436, only the O I 6158.2 Å line could be used, because the [O I] 6300.3 Å line is blended by a telluric O₂ line.

Sodium. The Na abundances were derived from the Na I 6154.2, 6160.8 Å doublet. The equivalent widths of these lines range from about 20 mÅ to 60 mÅ in our spectra. Non-LTE corrections were adopted from Lind et al. (2011) using the available IDL program to interpolate to the atmospheric parameters of the stars. The corrections of [Na/H] are negative reaching about -0.015 dex for the warmest stars in our sample. Although small, these corrections are not negligible in comparison with the statistical error of [Na/H]; from the comparison of the Na abundances derived from the two lines we find an average standard deviation of $\langle\sigma[\text{Na}/\text{H}]\rangle = 0.012$ dex.

Magnesium. The Mg abundances were obtained from the 4730.0 Å and 5711.1 Å Mg I lines of which the first have equivalent widths from 40 mÅ to 80 mÅ in our spectra, whereas the second line ranges from 80 mÅ to 120 mÅ. In order to obtain precise equivalent widths, this stronger line was measured with Voigt profile fitting instead of Gauss fitting.

Non-LTE corrections for the 5711.1 Å Mg I line were adopted from Osorio & Barklem (2016), who applied new quantum-mechanical calculations of cross sections for collisions with hydrogen (Barklem et al. 2012) and electrons (Osorio et al. 2015). The interactive database INSPECT¹ was used to interpolate to the stellar parameters resulting in corrections of [Mg/H] varying from being negligible for 16 Cyg A and B to about $+0.02$ dex for the warmest stars. Non-LTE corrections for the 4730.0 Å Mg I line are not available at INSPECT, but may be obtained with Spectrum Tools². The non-LTE data for Mg at this site are based on the model atoms and statistical-equilibrium calculations described in Bergemann et al. (2015, 2017), who also adopted quantum-mechanical hydrogen collisional rates from Barklem et al. (2012), but rates of electron collisions were calculated with classical formulae. Still, the differential non-LTE corrections of abundances derived from the 5711.1 Å Mg I line agree almost exactly with those of Osorio & Barklem (2016). The corrections of abundances obtained from the weaker 4730.0 Å line are about half the corrections for the 5711.1 Å line.

The abundances derived from the two Mg I lines show good agreement, that is $\langle\sigma[\text{Mg}/\text{H}]\rangle = 0.015$ dex.

Aluminium. The Al I 6696.0, 6698.7 Å doublet was used to derive Al abundances. In our spectra, the equivalent widths of these lines range from about 10 to 45 mÅ with the 6698.7 Å line being weaker than the 6696.0 Å line by about a factor of two. Non-LTE corrections were adopted from the statistical-equilibrium study by Nordlander & Lind (2017), who applied inelastic hydrogen-collisional rates of Belyaev (2013) for the six lower-excitation states of Al I. The corrections of [Al/H] are negligible for 16 Cyg A and B but rise to about $+0.040$ dex (for both lines) for our warmest stars.

Non-LTE corrections have also been published by Mashonkina et al. (2016, Table 2). Their data show a steeper rise of the corrections as a function of increasing T_{eff} leading

to a non-LTE correction of $+0.08$ dex for our warmest star. It is unclear what is causing the difference relative to Nordlander & Lind. Mashonkina et al. also applied the Belyaev (2013) cross sections, but since Nordlander & Lind used more realistic calculations for electron collisions than the formula of van Regemorter (1962) adopted by Mashonkina et al., we shall use the Nordlander-Lind corrections.

The comparison of Al abundances derived from the two Al I lines results in an average standard deviation of 0.016 dex for the eight stars with $T_{\text{eff}} > 6000$ K, nearly the same value as obtained for the C and Mg lines, but higher than in the case of Na.

Silicon. The Si abundances were determined from 7 - 10 high-excitation ($\chi_{\text{exc}} = 4.0 - 6.0$ eV) Si I lines with equivalent widths between 8 and 55 mÅ in our spectra. By comparing Si abundances derived from different lines we obtain $\langle\sigma[\text{Si}/\text{H}]\rangle = 0.020$ dex.

For the Si I lines at 5645.6 Å and 5665.6 Å, Spectrum Tools provides non-LTE corrections based on the statistical-equilibrium calculations of Bergemann et al. (2013) (see also Bergemann & Nordlander 2014). The differential corrections relative to the Sun are very small for our set of stars, at most -0.002 dex. As the other Si I lines have similar excitation potentials and equivalent widths, the non-LTE corrections are probably also small for these lines.

The calculations of Bergemann et al. (2013) are based on the semi-classical formula of Lambert (1993, Eq. A10) for the hydrogen-collisional rate. Mashonkina et al. (2016) have applied more advanced data from Belyaev et al. (2014) to calculate non-LTE corrections for Si I lines. They do not give numbers but state that the corrections are “vanishingly small” for solar-type stars. Furthermore, Amarsi & Asplund (2017) have applied the quantum-mechanical collisional rates of Belyaev et al. (2014) in a 3D non-LTE study of the Si abundance in the solar atmosphere. Several of our lines are included, and in agreement with Bergemann et al. (2013) they find a non-LTE correction of -0.01 dex only. Altogether, it seems safe to assume that we can neglect the differential non-LTE Si I corrections for our sample of stars.

Sulphur. For the solar twins, S abundances were determined from four high-excitation ($\chi_{\text{exc}} = 7.87$ eV) S I lines, which range in equivalent width from about 10 to 30 mÅ in our spectra. For the warmer stars, the abundance derived from the 6046.0 Å line has a systematic deviation of about -0.10 dex from the mean abundance of the other three lines. This is probably due to an unidentified blend in the line, which was therefore omitted. For the remaining three lines, the average standard deviation of the derived abundances is $\langle\sigma[\text{S}/\text{H}]\rangle = 0.033$ dex. This relatively high value can be ascribed to the weakness of the sulphur lines and difficulties in setting the continuum level. Still, the error of the mean value of [S/H] has a satisfactory low value of $\sigma_{\text{EW}}[\text{S}/\text{H}] = 0.019$ dex.

According to Takeda et al. (2005), the non-LTE corrections for the 6052.7 Å and 6757.1 Å S I lines are small (i.e. about -0.01 to -0.02 dex) and do not depend significantly on the atmospheric parameters of our stars. Therefore, differential corrections of S abundances relative to the Sun can be neglected. The 6743.6 Å line is not included by Takeda et al. (2005), but since this line belong to the same multiplet as the 6757.1 Å line, the non-LTE corrections are also expected so be negligible. We note, however, that the statistical-equilibrium calculations of Takeda et al. (2005) are based on cross sections for hydrogen collisions ac-

¹ <http://www.inspect-stars.com>

² <http://nlte.mpia.de>

ording to the Drawin formula. An update of the computations to quantum-mechanical cross sections would be desirable.

Calcium. Non-LTE calculations for Ca lines in spectra of late-type stars based on quantum-mechanical rates for Ca I + H I collisions have been carried out by Mashonkina et al. (2017). Four of our seven Ca I lines (5582.0 Å, 5590.1 Å, 6166.4 Å, and 6455.6 Å) are included. The average of the differential non-LTE corrections relative to the Sun are small, ranging from -0.007 dex to $+0.001$ dex for our set of stars. Assuming that the non-LTE corrections for the other three Ca I lines (5260.4 Å, 5513.0 Å, and 5867.6 Å) are also negligible small, it turns out that the 5513.0 Å line leads to systematically deviating abundances for stars with $T_{\text{eff}} > 6000$ K probably because a line from another element coincides with the Ca I line. Omitting this line, the Ca abundances derived from the other lines agree with an average standard deviation of $\langle \sigma[\text{Ca}/\text{H}] \rangle = 0.026$ dex.

Titanium. Ti abundances were derived from 11 Ti I and three Ti II lines. For the solar twins the equivalent widths range from about 10 to 60 mÅ, which is ideal for precise abundance determinations, but as the Ti I lines have low excitation potentials, several lines are very weak in the spectra of the warmest stars making the derived abundances uncertain. After excluding these lines, the average standard deviation becomes 0.028 dex for the Ti I lines, whereas it is 0.019 dex for the three Ti II lines

For all Ti I lines, *Spectrum Tools* provides non-LTE corrections based on the statistical-equilibrium calculations of Bergemann (2011). The corrections of $[\text{Ti}/\text{H}]_{\text{Ti I}}$ increase with increasing T_{eff} and decreasing $\log g$ reaching about $+0.03$ dex for our warmest and most evolved stars (KIC 7940546 and KIC 10162436). According to Bergemann (2011), non-LTE corrections for the Ti II lines are negligible and it is therefore interesting to compare Ti abundances derived from Ti I and Ti II lines. Assuming LTE, we get a mean difference $\langle [\text{Ti}/\text{H}]_{\text{Ti I}} - [\text{Ti}/\text{H}]_{\text{Ti II}} \rangle = -0.013 \pm 0.006$. Including the non-LTE corrections, the difference becomes $\langle [\text{Ti}/\text{H}]_{\text{Ti I}} - [\text{Ti}/\text{H}]_{\text{Ti II}} \rangle = +0.002 \pm 0.004$, that is a better agreement. Considering the errors, this is not a proof of the validity of the non-LTE corrections, but we conclude that there is a very satisfactory agreement between abundances derived from Ti I and Ti II lines supporting the T_{eff} values derived by requesting that Fe abundances derived from Fe I and Fe II lines should be the same when adopting the seismic $\log g$ value (see Sect. 3.1).

Chromium. Cr abundances were derived from 6 - 8 Cr I and two Cr II lines. There is no systematic calculations of non-LTE corrections as a function of T_{eff} and $\log g$ for solar-type stars, but Bergemann & Cescutti (2010) have presented a non-LTE study of Cr abundances in the Sun and some metal-poor stars. Neglecting collisions with hydrogen atoms, they found quite large non-LTE corrections for the Sun, that is $+0.05$ to $+0.10$ dex for our Cr I lines, whereas the corrections for the Cr II lines are negligible.

Although new statistical-equilibrium calculations including hydrogen collisions according to the Drawin formula by Scott et al. (2015) lead to smaller corrections for solar Cr I lines (~ 0.025 dex), differential corrections relative to the Sun may be significant for our warmer stars. To check this we have compared Cr abundances derived from Cr I and Cr II lines. For 16 Cyg A and B there is almost perfect agreement, but for the other stars we find a mean difference $\langle [\text{Cr}/\text{H}]_{\text{Cr I}} - [\text{Cr}/\text{H}]_{\text{Cr II}} \rangle = -0.014 \pm 0.007$. Assuming this is due to non-LTE effects, we have added 0.014 dex to the abundances derived from Cr I lines and calculated a mean Cr abundance from the Cr I and Cr II lines

giving equal weight to all lines. The resulting average standard deviation of $[\text{Cr}/\text{H}]$ is 0.029 dex.

Iron. As discussed in Sect. 3.1, the non-LTE corrections of Lind et al. (2012) are negligible for Fe II lines but reach about $+0.02$ dex for Fe I lines in the spectra of our warmest stars. Because effective temperatures were derived so that the same Fe abundance is obtained from Fe I and Fe II lines, and because there are many more Fe I lines ($N_{\text{lines}} = 40$ to 47) than Fe II lines ($N_{\text{lines}} = 8$ or 9), the error of $[\text{Fe}/\text{H}]$ arising from the equivalent width measurements gets the largest contribution from the Fe II lines. The average standard deviation is nearly the same for Fe I and Fe II lines, 0.021 dex and 0.022 dex, respectively.

Nickel. The Ni abundances were determined from 10 to 14 Ni I lines having equivalent widths between 5 and 100 mÅ. From the the line-to-line scatter of $[\text{Ni}/\text{H}]$ we find an average standard deviation of 0.021 dex, which is the same as obtained for the Fe I lines.

Unfortunately, there are no non-LTE calculations for nickel. In their determination of the photospheric Ni abundance for the Sun, Scott et al. (2015) argue that non-LTE corrections are small, which is supported by the fact that they find agreement between the derived solar abundance, $A(\text{Ni}) = 6.20 \pm 0.04$, and the meteoritic abundance $A(\text{Ni}) = 6.20 \pm 0.01$ (Lodders et al. 2009). However, it cannot be excluded that there are small non-LTE corrections on the Ni abundances of the *Kepler* stars. Ni I has about the same ionization potential and a similar energy level structure as Fe I, so it would not be surprising if the non-LTE corrections are of the same order of size.

Zinc. Zn abundances were derived from two medium-strong Zn I lines at 4722.2 Å and 4810.5 Å and a weak Zn I line at 6362.4 Å. Non-LTE corrections with hydrogen-collisional rates according to the Drawin formula have been calculated by Takeda et al. (2005). The correction of $[\text{Zn}/\text{H}]$ reaches a maximum of about $+0.03$ dex for the stronger lines, but only $+0.01$ dex for the 6362.4 Å line. After applying these corrections, the average standard deviation of the abundances derived from the three lines is 0.033 dex. This is higher than for most elements, which is probably due to difficulties in setting the continuum level for the blue lines.

Yttrium. Three Y II lines at 4883.7, 5087.4, and 5200.4 Å were used to determine Y abundances. The equivalent widths of the strongest line (4883.7 Å) range from 60 mÅ to 74 mÅ and those of the weakest line (5200.4 Å) from 38 mÅ to 46 mÅ for our sample of stars. Non-LTE studies are not available, but since the single-ionized state is by far the most populated, we expect corrections for Y II lines to be small as in the case of the Ti II, Cr II, and Fe II lines, but this should be investigated in more detail.

Yttrium is an odd-Z element, so hyperfine structure (HFS) is present in the spectral lines. However, as discussed by Hannaford et al. (1982) in their determination of the solar Y abundance, the HFS splitting is less than 1 mÅ. This is a factor 3 to 4 smaller than the Doppler width of the Y II lines due to thermal broadening and microturbulence. Therefore, we have neglected HFS effects when deriving $[\text{Y}/\text{H}]$.

The Y abundances derived from the three lines agree very well; the average standard deviation of $[\text{Y}/\text{H}]$ is 0.016 dex close to that of Mg and Al. This high precision is important, because the Y/Mg and Y/Al ratios are applied to study the Galactic evolution of a typical *s*-process element as discussed in Sect. 4.

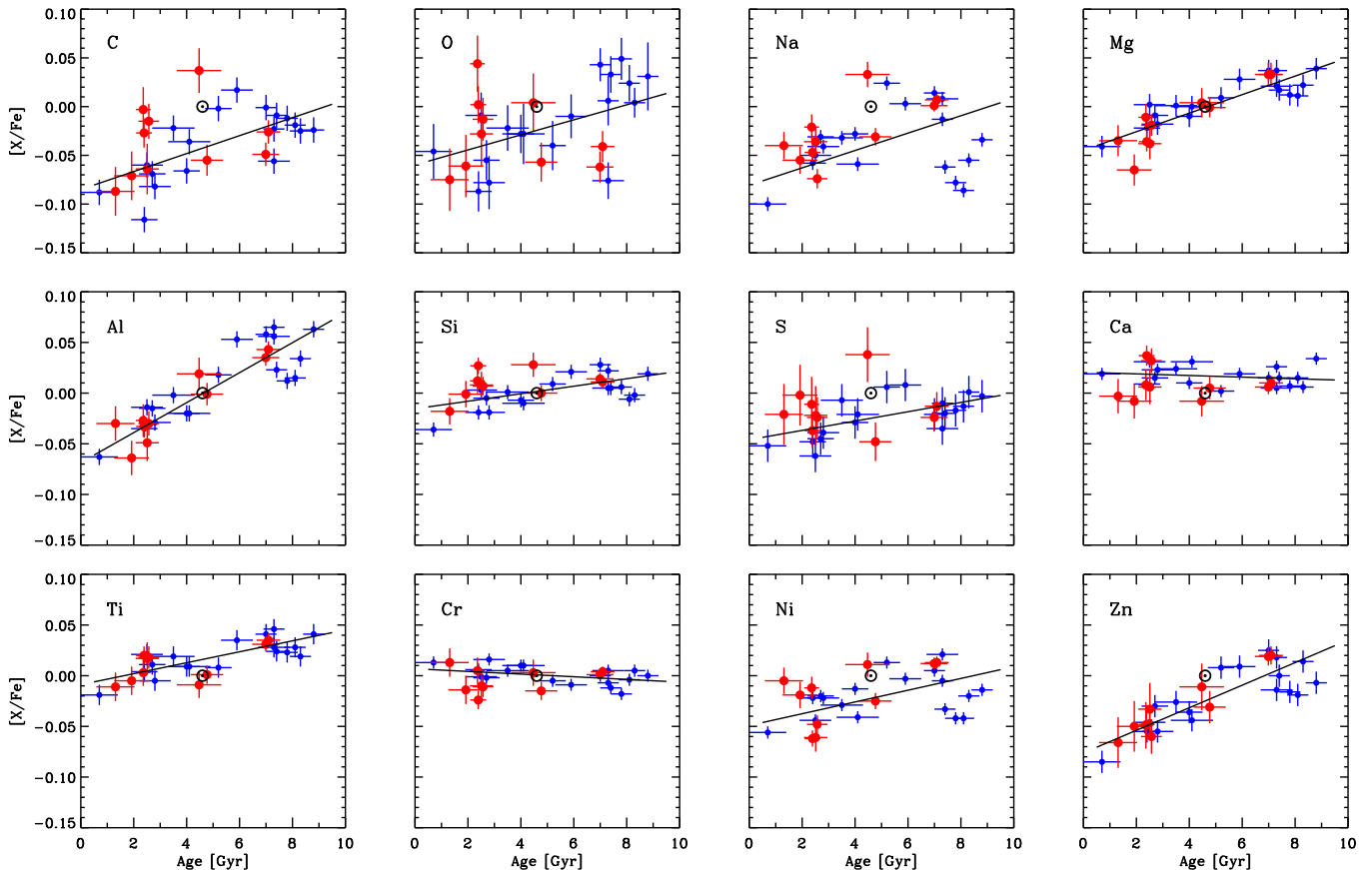


Fig. 3. Abundance ratios $[X/Fe]$ as a function of stellar age. Large (red) filled circles refer to *Kepler* LEGACY stars and small (blue) filled circles to solar twins from Nissen (2015). The lines show maximum likelihood linear fits to the data with errors in both coordinates taken into account. The Sun, shown with the \odot symbol, was not included in the fits. Zero points and slope coefficients for the fits are given in Table 3.

3.2.2. 3D effects and systematic errors

Studies of non-LTE effects on derived stellar abundances have progressed considerably in recent years as discussed above. Still, it is only in the case of oxygen that full 3D non-LTE calculations on an extensive grid of stellar parameters have been carried out (Amarsi et al. 2016a). Although the 3D non-LTE corrections for the $[O/H]$ abundances derived from the 6158.2 Å and 6300.3 Å lines are small for our sample of stars, it could be that full 3D non-LTE calculations for the other elements will lead to significant changes of the derived abundances.

An associated problem is the microturbulent broadening of spectral lines. For the 1D models, we assume that it can be described by a single parameter determined so that $[Fe/H]$ from Fe I lines has no systematic dependence on equivalent width, but in real stellar atmospheres, the microturbulence probably depends on depth. If element abundances are based on weak lines on the linear part of the curve of growth (C, O, Na, Al, Si, and S in our case) this is not a significant problem, but if stronger lines on the flat part of the curve of growth are involved (Mg, Ca, Ti, Cr, Ni, Zn, and Y) a variation of microturbulence with atmospheric depth may affect the derived $[X/Fe]$ values. Hydrodynamical models will take care of this problem, but 3D non-LTE studies are computationally very demanding and beyond the scope of this paper. As further discussed in Sect. 4.1 we may, however, get an empirical check of the importance of the 3D ef-

fects by comparing $[X/Fe]$ values for stars having similar ages but different effective temperatures; as $[X/Fe]$ is measured relative to the Sun, one would expect to see the largest 3D effects for the warmest stars in our sample.

Variations in stellar activity among stars of similar age is another potential problem when determining high-precision stellar abundances. Flores et al. (2016) have discovered that one of the solar twins included in Paper I, HD 45184, has a 5.14 yr activity cycle over which the equivalent widths of strong Fe II lines change with an amplitude of about ± 1 mÅ, and Reddy & Lambert (2017) have shown that derived $[Ba/Fe]$ values of young solar twins are positively correlated with the Ca II stellar activity index. They suggest that the very high $[Ba/Fe]$ values derived for stars in young open clusters (D’Orazi et al. 2009) are not real but due to an underestimation of the microturbulence in the upper photospheric layers of active stars, where the Ba II 5853.7 Å line used to determine Ba abundances is formed. Although our Y II lines are weaker than the Ba II 5853.7 Å line and formed in deeper layers, we cannot exclude that this problem also has some effect on the derived yttrium abundances and hence on the $[Y/Mg]$ -age relation discussed in Sect. 4.1.

Table 2. [Fe/H] and [X/Fe] for 13 elements.

ID	[Fe/H]	σ	[C/Fe]	σ	[O/Fe]	σ	[Na/Fe]	σ	[Mg/Fe]	σ	[Al/Fe]	σ	[Si/Fe]	σ
KIC 3427720	-0.024	0.017	-0.003	0.023	0.044	0.029	-0.021	0.013	-0.011	0.014	-0.027	0.016	0.012	0.012
KIC 6106415	-0.037	0.012	-0.055	0.016	-0.057	0.020	-0.031	0.009	-0.001	0.010	-0.001	0.011	0.000	0.008
KIC 6225718	-0.110	0.014	-0.015	0.018	-0.013	0.022	-0.074	0.010	-0.019	0.011	-0.030	0.012	0.007	0.009
KIC 7940546	-0.126	0.012	-0.027	0.015	0.002	0.019	-0.047	0.009	-0.036	0.010	-0.033	0.011	0.027	0.008
KIC 9139151	0.096	0.019	-0.071	0.025	-0.061	0.032	-0.055	0.014	-0.065	0.016	-0.064	0.017	-0.001	0.013
KIC 10162436	-0.073	0.021	-0.064	0.026	-0.028	0.033	-0.036	0.015	-0.038	0.016	-0.049	0.018	0.008	0.013
KIC 10644253	0.130	0.019	-0.087	0.025	-0.075	0.032	-0.040	0.014	-0.035	0.016	-0.030	0.017	-0.018	0.013
16 Cyg A	0.093	0.007	-0.049	0.012	-0.062	0.016	0.001	0.006	0.033	0.012	0.035	0.008	0.014	0.006
16 Cyg B	0.062	0.007	-0.026	0.012	-0.041	0.016	0.007	0.006	0.033	0.012	0.043	0.008	0.011	0.006
KIC 12258514	0.027	0.017	0.037	0.023	0.004	0.030	0.033	0.013	0.004	0.015	0.019	0.016	0.028	0.012
ID	[S/Fe]	σ	[Ca/Fe]	σ	[Ti/Fe]	σ	[Cr/Fe]	σ	[Ni/Fe]	σ	[Zn/Fe]	σ	[Y/Fe]	σ
KIC 3427720	-0.011	0.027	0.008	0.015	0.003	0.013	0.005	0.013	-0.012	0.011	-0.049	0.023	-0.006	0.015
KIC 6106415	-0.048	0.019	0.005	0.011	0.001	0.009	-0.015	0.009	-0.025	0.008	-0.031	0.016	0.001	0.011
KIC 6225718	-0.024	0.020	0.032	0.012	0.018	0.011	-0.011	0.010	-0.048	0.009	-0.060	0.017	0.032	0.012
KIC 7940546	-0.037	0.017	0.037	0.010	0.020	0.009	-0.024	0.009	-0.062	0.008	-0.048	0.015	0.020	0.010
KIC 9139151	-0.002	0.030	-0.008	0.017	-0.005	0.014	-0.014	0.014	-0.019	0.013	-0.050	0.025	0.036	0.017
KIC 10162436	-0.022	0.029	0.006	0.017	0.017	0.016	-0.010	0.015	-0.061	0.014	-0.033	0.026	0.033	0.018
KIC 10644253	-0.021	0.030	-0.003	0.017	-0.011	0.014	0.013	0.014	-0.005	0.013	-0.066	0.025	0.031	0.017
16 Cyg A	-0.024	0.014	0.006	0.007	0.031	0.007	0.001	0.005	0.012	0.006	0.019	0.009	-0.057	0.007
16 Cyg B	-0.013	0.014	0.010	0.007	0.035	0.007	0.004	0.005	0.013	0.006	0.020	0.009	-0.052	0.007
KIC 12258514	0.038	0.027	-0.008	0.015	-0.009	0.013	0.003	0.013	0.011	0.012	-0.011	0.023	-0.047	0.016

4. Discussion

The derived [X/Fe] values of the *Kepler* stars are given in Table 2. The listed errors are a combination of the errors arising from the measurement of equivalent widths as estimated from the line-to-line scatter, (see Sect. 3.2.1) and the errors arising from the uncertainties in T_{eff} , $\log g$, [Fe/H], and ξ_{turb} .

Stellar ages from Silva Aguirre et al. (2017) are given in Table 1. For each star, the age is calculated as the mean of the results from the seven different analyses of the available seismic data. The age error is calculated as a quadratic combination of the mean of the errors estimated for the seven analyses and the standard deviation resulting from a comparison of ages of the different analyses. In this way, we take into account both the statistical error due to uncertainties of the measured oscillation frequencies and the systematic uncertainty arising from the analysis method.

The ages of the *Kepler* LEGACY stars derived in Silva Aguirre et al. (2017) are primarily based on the observed oscillation frequencies but constraints on T_{eff} and [Fe/H] are also included in the analysis. These parameters were taken from Buchhave & Latham (2015) and assumed to have errors of ± 77 K and ± 0.1 dex, respectively, except in the case of 16 Cyg A and B for which more precise values from Ramírez et al. (2009) were adopted. For all stars our metallicities agree with those used in Silva Aguirre et al. (2017) within their one-sigma uncertainty, but for three stars, KIC 7940546, KIC 9139151, and KIC 10162436, our T_{eff} values deviate with 91 K, -187 K, and 115 K, respectively. In order to see if the new values of T_{eff} and [Fe/H] have any significant impact on the ages derived, we have repeated the age determinations for the ASTFIT (Christensen-Dalsgaard 2008a,b) and BASTA (Silva Aguirre et al. 2015) analysis methods. In both cases, the improved spectroscopic parameters lead to age changes having an rms deviation of only 0.2 Gyr relative to the ages determined

Table 3. Linear fits of [X/Fe] as a function of stellar age.

	a [dex]	b 10^{-3} dex Gyr $^{-1}$	χ_{red}^2
[C/Fe]	-0.085 ± 0.009	$+9.2 \pm 1.7$	3.6
[O/Fe]	-0.060 ± 0.013	$+7.7 \pm 2.4$	3.1
[Na/Fe]	-0.081 ± 0.016	$+8.9 \pm 2.5$	16.8
[Mg/Fe]	-0.045 ± 0.004	$+9.5 \pm 0.7$	1.1
[Al/Fe]	-0.069 ± 0.007	$+14.8 \pm 1.1$	2.7
[Si/Fe]	-0.015 ± 0.004	$+3.7 \pm 0.7$	3.0
[S/Fe]	-0.046 ± 0.006	$+4.6 \pm 1.0$	1.0
[Ca/Fe]	$+0.021 \pm 0.003$	-0.8 ± 0.3	2.1
[Ti/Fe]	-0.009 ± 0.004	$+5.4 \pm 0.6$	1.1
[Cr/Fe]	$+0.007 \pm 0.003$	-1.3 ± 0.5	1.8
[Ni/Fe]	-0.049 ± 0.008	$+5.8 \pm 1.2$	8.9
[Zn/Fe]	-0.077 ± 0.006	$+11.2 \pm 0.9$	1.8

in Silva Aguirre et al. (2017), and for all stars the age change is less than the age error given in Table 1.

4.1. [X/Fe]- age correlations

Fig. 3 shows [X/Fe] as a function of stellar age for the ten *Kepler* LEGACY stars and 18 solar twins from Paper I (excluding three α -enhanced stars). For the solar twins, we have adopted isochrone ages determined from evolutionary tracks in the $\log g$ - T_{eff} diagram calculated with the Aarhus Stellar Evolution Code, ASTEC (see Nissen 2016). Linear fits ($[X/Fe] = a + b \cdot \text{Age}$) to all data were determined by a maximum likelihood program that includes errors in both coordinates (Press et al. 1992). The coefficients a and b and the reduced chi-squares of the fits are given in Table 3.

As seen from Fig. 3, the *Kepler* stars have similar dependencies of $[X/Fe]$ on age as the solar twins, albeit with a larger scatter due to larger errors of $[X/Fe]$. We also note that the deviations of $[X/Fe]$ from the fitted lines do not have any significant dependence on T_{eff} , suggesting that 3D effects are not important for the derived age trends (see Sect. 3.2.2).

Among the element ratios shown in Fig. 3, $[Mg/Fe]$, $[Al/Fe]$, and $[Zn/Fe]$ have particular tight trends as a function of stellar age. Over the lifetime of the Galactic disk, these abundance ratios decrease by about 0.1 dex. Given that Mg, Al, and Zn are exclusively made in Type II supernovae (SNe), whereas Fe is also produced by Type Ia SNe (e.g. Kobayashi et al. 2006), this can be explained as due to an increasing number of Type Ia SNe relative to the number of Type II SNe in the course of time. $[Si/Fe]$, $[S/Fe]$, and $[Ti/Fe]$ also increase with stellar age, but the amplitude of the variations is smaller (~ 0.05 dex), because Si, S, and Ti have some contribution from Type Ia SNe in addition to the Type II SNe contribution (Kobayashi et al. 2006). $[Ca/Fe]$ and $[Cr/Fe]$, on the other hand, are nearly constant with age. While this is expected for $[Cr/Fe]$, the constancy of $[Ca/Fe]$ is surprising. As discussed in Paper I, the explanation may be that low luminosity SNe producing large amounts of Ca (Perets et al. 2010) are important for the chemical evolution of Ca.

$[C/Fe]$, $[O/Fe]$, $[Na/Fe]$, and $[Ni/Fe]$ also increase as a function of age, but the scatter is larger than expected from the estimated errors of $[X/Fe]$ and age, that is $\chi_{\text{red}}^2 > 3$ as seen from Table 3. In the case of Na and Ni, the large scatter is mainly due to the existence of five old stars with low values of $[Na/Fe]$ and $[Ni/Fe]$. The origin of such stars and a possible explanation of a tight correlation between $[Ni/Fe]$ and $[Na/Fe]$ are discussed in Paper I.

The scatter in $[C/Fe]$ and $[O/Fe]$ is probably related to variations in the ratio between volatile and refractory elements at a given age. Such variations were revealed by Meléndez et al. (2009), who compared $[X/Fe]$ for the Sun as a function of the elemental condensation temperature, T_c , in a solar composition gas (Lodders 2003) with the corresponding trend for eleven solar twins having ages similar to the age of the Sun. The Sun was found to have a higher volatile-to-refractory ratio than most of the twins, which may be due to sequestration of refractory elements in the terrestrial planets of the solar system (Meléndez et al. 2009) or dust-gas segregation in star-forming clouds (Önehag et al. 2014; Gaidos 2015). Other examples of variations in the volatile-to-refractory ratio (or the $[X/H] - T_c$ slope) between stars of similar age are presented by Spina et al. (2016b) in a high-precision study of 14 solar twins. Differences of the $[X/H] - T_c$ slope are also seen between twin stars in binary systems (e.g. Tucci Maia et al. 2014; Teske et al. 2016a,b; Saffe et al. 2017), which is particularly interesting, because dust-gas segregation before planet formation is likely to affect the abundances of the two components in the same way making it more likely that the observed abundance differences are due to planet-star interactions.

In our sample of *Kepler* stars, KIC 6106415 and KIC 12258514 provide an interesting case. The two stars have about the same age as the Sun (4.8 ± 0.6 Gyr and 4.5 ± 0.8 Gyr, respectively), but as seen from Fig. 4, the $[X/H]-T_c$ slopes are very different: $+4.0 \pm 0.6 \cdot 10^{-5}$ dex K^{-1} for KIC 6106415 and $-2.2 \pm 1.1 \cdot 10^{-5}$ dex K^{-1} for KIC 12258514. Such variations make a large contribution to the scatter in the age relations for $[C/Fe]$ and $[O/Fe]$, and also add to the scatter in age relations of other volatile elements (Na, S, and Zn), whereas abundance ratios between refractory elements (e.g. $[Mg/Fe]$) are not significantly affected.

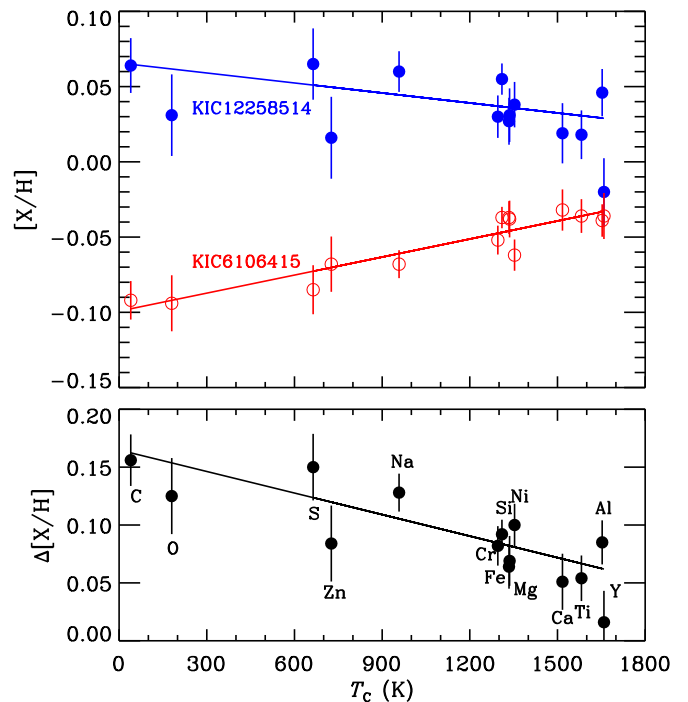


Fig. 4. Comparison of the $[X/H]-T_c$ relations for KIC 6106415 and KIC 12258514. The lower panel shows the difference in $[X/H]$ between KIC 12258514 and KIC 6106415. The lines show weighted least-squares fits to the data.

A particularly strong age dependence is found for the ratios between the s -process element yttrium and the α -capture elements magnesium and aluminium. As seen from Fig. 5, the *Kepler* stars confirm the age trends of $[Y/Mg]$ and $[Y/Al]$ previously found for solar twins (Nissen 2016). Maximum likelihood fits to all stars (excluding the Sun) with errors in both coordinates taken into account give

$$[Y/Mg] = 0.150 (\pm 0.007) - 0.0347 (\pm 0.0012) \text{ Age [Gyr]}, \quad (1)$$

and

$$[Y/Al] = 0.174 (\pm 0.008) - 0.0400 (\pm 0.0012) \text{ Age [Gyr]}. \quad (2)$$

In both cases, the reduced chi-square of the fit is 1.2, and the slope coefficients are similar to those determined for solar twins alone (Nissen 2016; Spina et al. 2016a).

The strong increase of Y/Mg and Y/Al with decreasing stellar age, about 0.3 dex over the lifetime of the Galactic disk, may be explained by production of yttrium via the slow neutron-capture process in low-mass ($1-4 M_{\text{Sun}}$) asymptotic-giant-branch (AGB) stars (e.g. Travaglio et al. 2004; Karakas & Lugaro 2016). As time goes on, an increasing number of low-mass stars reach the AGB phase, whereas the number of type II SNe producing Mg and Al declines. It should, however, be emphasized that the tight relations shown in Fig. 5 were obtained for stars selected to have metallicities in the range $-0.15 < [Fe/H] < +0.15$. Feltzing et al. (2017) have shown that $[Y/Mg]$ decreases with $[Fe/H]$ at a given age. This makes sense, because at lower metallicity there are fewer Fe atoms per neutron to act as seeds for the s -process. Hence, the use of $[Y/Mg]$ (or $[Y/Al]$) as a clock to measure stellar ages requires a calibration that includes a metallicity term.

The tight relations between stellar age and abundance ratios such as Mg/Fe and Y/Mg stand out in contrast to the lack of

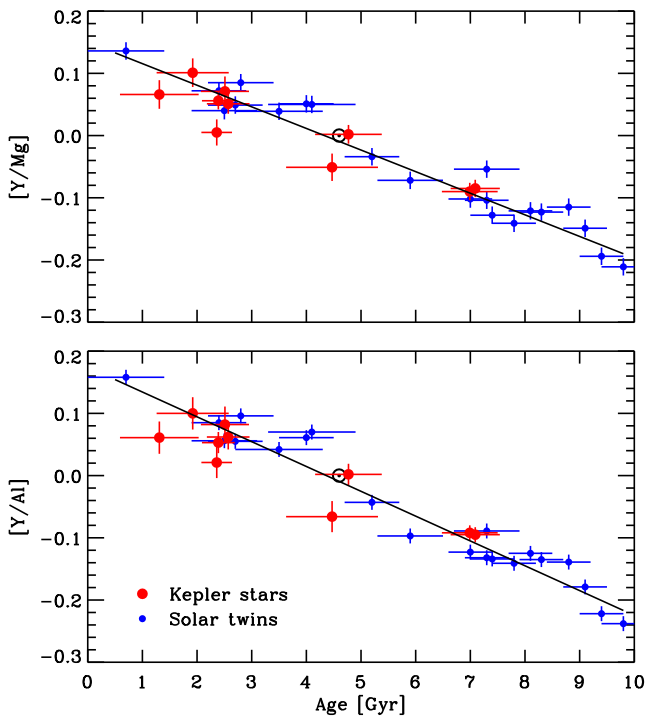


Fig. 5. $[Y/Mg]$ and $[Y/Al]$ versus stellar age for *Kepler* LEGACY stars and solar twins including three α -enhanced with ages between 9 and 10 Gyr. The lines show the linear fits corresponding to Eqs. (1) and (2).

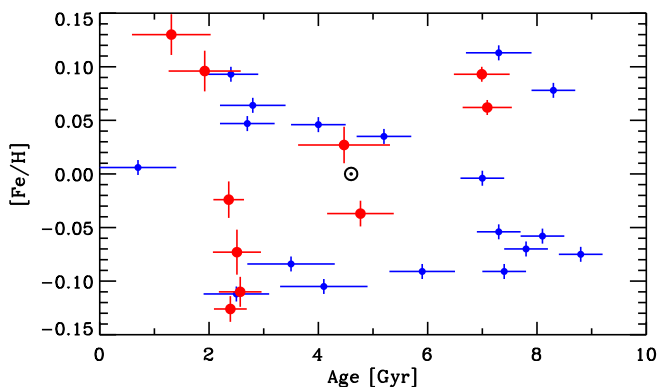


Fig. 6. $[Fe/H]$ versus stellar age for *Kepler* LEGACY stars (large red filled circles) and solar twins (small blue filled circles).

correlation between $[Fe/H]$ and age (see Fig. 6). The scatter in the age-metallicity relation for stars in the solar neighbourhood³ is often explained as due to radial mixing of stars in a Galactic disk with a gradient in $[Fe/H]$; stars presently in the solar neighbourhood were born at different Galactocentric distances (R_G). However, in order to explain the low scatter in Mg/Fe and Y/Mg at a given age, the gradients in these abundance ratios should then be vanishingly small at all times, which requires that the ratios between the number of Type II SNe, Type Ia SNe, and AGB stars have evolved in the same way independent of R_G . This corresponds to a weak or non-existent inside-out formation history of the Galactic disk (Haywood et al. 2015).

³ According to Gaia DR1 parallaxes (Gaia Collaboration et al. 2016a,b) all *Kepler* stars included in this paper have distances less than 140 pc.

Table 4. Comparison of atmospheric parameters and $[Fe/H]$ for 16 Cyg A and B between Tucci Maia et al. (2014) and this paper.

	16 Cyg A	16 Cyg B
T_{eff}^a	5830 ± 11 K	5751 ± 11 K
T_{eff}^b	5816 ± 10 K	5763 ± 10 K
$\log g^a$	4.300 ± 0.02	4.350 ± 0.02
$\log g^b$	4.291 ± 0.01	4.356 ± 0.01
$[Fe/H]^a$	0.101 ± 0.008	0.054 ± 0.008
$[Fe/H]^b$	0.093 ± 0.007	0.062 ± 0.007

Notes. ^(a) Tucci Maia et al. (2014). ^(b) This paper.

4.2. 16 Cyg A and B

Among the *Kepler* stars included in this paper, the two components of the 16 Cyg binary system are of particular interest. The very detailed set of oscillation frequencies for these relatively bright stars has made it possible to derive precise values of masses, radii and ages (Metcalf et al. 2015), helium abundances (Verma et al. 2014), and rotation periods (Davies et al. 2015). Furthermore, a comparison of the seismic radii with those determined from interferometric angular diameters (White et al. 2013) provides an important test of asteroseismology (see Silva Aguirre et al. 2017).

The chemical compositions of 16 Cyg A and B are also very interesting. Cochran et al. (1997) discovered that 16 Cyg B has a Jupiter-sized planet with a mass $M > 1.5M_{\text{Jup}}$ in an eccentric orbit with a period of 800 days, whereas no planets have been detected around 16 Cyg A. Hence, a comparison of abundances of the two stars has the potential of revealing possible effects of planet formation or planet accretion on stellar surface composition as discussed by Laws & Gonzalez (2001), who in a high-precision spectroscopic analysis found a small metallicity difference, $\Delta[Fe/H]$ ($A - B$) = 0.025 ± 0.009 , between 16 Cyg A and B. This was supported by Ramírez et al. (2011), who found systematic differences of the abundances of the two components corresponding to a mean difference of $\langle \Delta[X/H] \rangle$ ($A - B$) = 0.041 ± 0.007 for 22 elements. However, in a similar study by Schuler et al. (2011), the mean abundance difference for 15 elements was found to be only 0.003 ± 0.015 dex.

In order to clarify the controversy about the chemical compositions of 16 Cyg A and B, Tucci Maia et al. (2014) made a new high-precision spectroscopic analysis using CFHT/ESPaDONs spectra with $R = 81\,000$ and $S/N = 700$. From a strictly differential analysis of the two stars, they obtained $\Delta[Fe/H]$ ($A - B$) = 0.047 ± 0.005 supporting the abundance difference found by Ramírez et al. (2011). Furthermore, they found the abundance difference between A and B to increase with elemental condensation temperature for the refractory elements, and interpreted this as a signature of sequestration of refractory elements in the core of the giant planet around 16 Cyg B.

The atmospheric parameters and abundances of 16 Cyg A and B derived in this paper from HARPS-N spectra with $R = 115\,000$ and $S/N \approx 800$ support the results of Tucci Maia et al. (2014). As seen from Table 4, the derived values of T_{eff} , $\log g$, and $[Fe/H]$ agree within the estimated one-sigma errors. In particular, there is a remarkable agreement between the gravities considering that Tucci Maia et al. (2014) used the ionization equilibrium of Fe to obtain $\log g$, whereas our values are derived from seismic data. Our A–B difference in T_{eff} (53 K) is somewhat smaller than that of Tucci Maia et al. (79 K), which leads

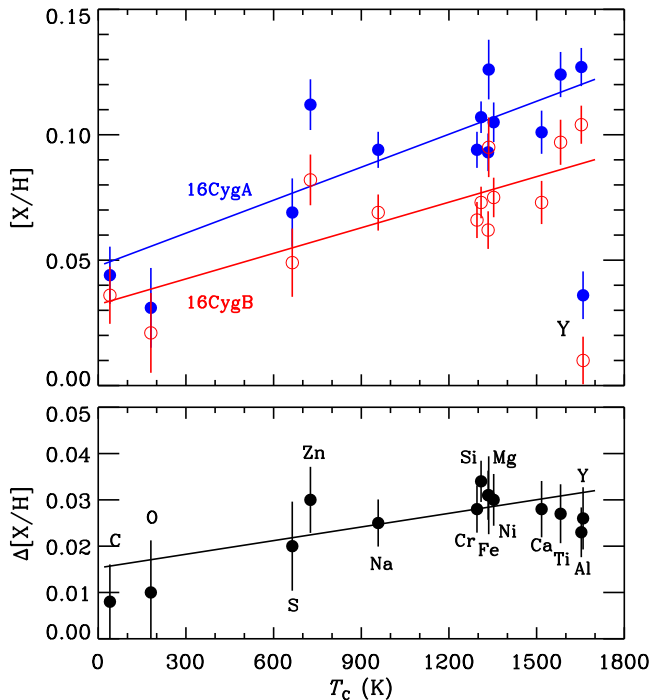


Fig. 7. $[X/H]$ values of 16 Cyg A and B versus elemental condensation temperature. The lower panel shows the difference in $[X/H]$ between A and B. The lines show weighted least-squares fits to the data (excluding yttrium).

to a smaller difference in $[Fe/H]$, but our difference $\Delta[Fe/H]$ ($A - B$) = 0.031 ± 0.010 is still significant at the three-sigma level. There is also good agreement between the abundances of 13 elements in common between the two works. The $[X/H]$ -values agree within about one-sigma of the combined errors, except in the case of oxygen, for which the $[O/H]$ values derived by Tucci Maia et al. are about 0.05 dex larger than our values.

As seen from Fig. 7, the $[X/H]$ values of 16 Cyg A and B show an increasing trend as a function of the condensation temperature for the elements, as also found by Tucci Maia et al. (2014). The scatter around the fitted lines is, however, larger than expected from the estimated errors. Large deviations are seen for Mg, Al, Zn, and in particular Y, that is the elements for which $[X/Fe]$ has the steepest dependence on stellar age. Hence, the scatter is probably due to the age difference between the Sun and the 16 Cyg system. Interestingly, the difference in $[X/H]$ between 16 Cyg A and 16 Cyg B (lower panel of Fig. 7) has a much tighter correlation with condensation temperature, and increase with increasing T_c at a slope of $+0.98 \pm 0.35 \cdot 10^{-5} \text{ dex K}^{-1}$. In comparison, Tucci Maia et al. (2014) found a $\Delta[X/H]$ ($A-B$) T_c -slope of $+1.88 \pm 0.79 \cdot 10^{-5} \text{ dex K}^{-1}$ for refractory elements with $T_c > 900 \text{ K}$. Our slope is smaller but refers to the whole T_c -range⁴.

While the abundance differences between 16 Cyg A and B discussed above are small, there is a much larger difference for lithium (e.g. King et al. 1997; Ramírez et al. 2011). As shown by Carlos et al. (2016), 16 Cyg B lie on the $A(\text{Li})$ -age relation for the large majority of solar twins, but 16 Cyg A lie about 0.6 dex above this relation. According to Deal et al. (2015), the small

mass difference between A and B cannot explain the difference in $A(\text{Li})$. As discussed by Melendez & Ramirez (2016), the difference could, however, be due to a recent accretion by 16 Cyg A of a Jupiter-sized planet in which the original amount of Li had been retained, whereas 16 Cyg B has not been exposed to such accretion. This scenario may also explain the enhancement of heavier elements in 16 Cyg A relative to 16 Cyg B. More detailed studies are, however, needed; Deal et al. (2015) argue that fingering convection induced by accretion of heavy elements will transport Li down to nuclear destruction layers and dilute the pollution by heavy elements.

5. Conclusions and outlook

With the aim of testing trends of abundance ratios versus stellar age as previously revealed for solar twins, we have used HARPS-N spectra with $S/N \gtrsim 250$ to derive high-precision abundances for ten *Kepler* LEGACY stars having ages determined from asteroseismology (Silva Aguirre et al. 2017). The seismic data have also been used to determine precise values of stellar gravities, which allowed us to derive effective temperatures from the ratio between equivalent widths of Fe I and Fe II lines.

The abundances were derived by an LTE analysis of spectral lines using MARCS 1D model atmospheres. For the ranges of atmospheric parameters covered by the stars ($5750 < T_{\text{eff}} < 6350 \text{ K}$, $3.95 < \log g < 4.40$, and $-0.15 < [Fe/H] < +0.15$) differential non-LTE corrections of abundances relative to those of the Sun cannot be neglected. Thanks to recent progress in non-LTE studies such corrections are available for many of the elements included as discussed in Sect. 3.2.1. The largest corrections of $[X/H]$ for our sample of stars are typically 0.02 to 0.04 dex, which is of the same order of size as the precision of the abundances derived. In addition to this, there may also be significant differential 3D corrections, but these are only available in the case of oxygen (Amarsi et al. 2016a). Hence, 3D non-LTE studies for other elements would be highly interesting to further improve the accuracy of the abundance determinations. Effects of stellar activity (Flores et al. 2016; Reddy & Lambert 2017) on abundance determinations also deserve further studies.

We also note that atomic diffusion of elements (gravitational settling and radiative acceleration) changes stellar surface abundances as a function of time. According to the stellar evolution models of Dotter et al. (2017), which include turbulent mixing and convective overshoot, $[Fe/H]$ of solar-type stars with $T_{\text{eff}} < 6000 \text{ K}$ decreases by approximately 0.10 dex as the age increases from zero to 10 Gyr, whereas $[Mg/Fe]$ increases by ~ 0.01 dex. Hence, diffusion cannot be neglected if we want accurate information on Galactic chemical evolution or abundances at stellar birth. Further studies of the change of stellar surface abundances as a function of age is much needed especially for $T_{\text{eff}} > 6000 \text{ K}$, where the effect of diffusion depends critically on whether one includes radiative acceleration or not (Dotter et al. 2017, Fig. 9).

The abundances of the *Kepler* stars confirm the trends between $[X/Fe]$ and stellar age previously found for solar twins (see Fig. 3). For Mg, Al, Si, Ca, Ti, Cr, Zn, and Y, the scatter in $[X/Fe]$ around fitted linear relations in an age interval from 1 to 9 Gyr is of the same order of size as the errors of the $[X/Fe]$ abundance ratios, that is 0.01 - 0.02 dex for solar twins and 0.02 - 0.03 dex for *Kepler* stars. This small scatter stands out in contrast to a scatter of about 0.1 dex in $[Fe/H]$ (see Fig. 6). Often the scatter in the age-metallicity relation for the solar neighbourhood is explained by radial mixing in a Galactic disk formed inside-out causing a gradient in $[Fe/H]$ (e.g. Minchev et al. 2013,

⁴ Based on new spectra of 16 Cyg A and B with $R \sim 160\,000$ and $S/N \sim 700$, Tucci Maia et al. (2017) obtain a $\Delta[X/H]$ ($A-B$) T_c -slope of $+1.48 \pm 0.25 \cdot 10^{-5} \text{ dex K}^{-1}$ for the whole T_c -range in better agreement with our result.

2014), but it remains to be seen if such models can explain the small scatter of for example $[\text{Mg}/\text{Fe}]$ and $[\text{Y}/\text{Mg}]$. As an alternative explanation of the scatter in the age-metallicity relation, Edvardsson et al. (1993) suggest infall of metal-poor gas clouds onto the Galactic disk followed by stars formation before mixing evens out the inhomogeneities in $[\text{Fe}/\text{H}]$. If the clouds are sufficiently poor in metals, that is $[\text{Fe}/\text{H}]$ and $[\text{Mg}/\text{H}] < -1$, infall coupled with star formation could cause a scatter of 0.1 dex in $[\text{Fe}/\text{H}]$ (and $[\text{Mg}/\text{H}]$), but less than 0.01 dex in $[\text{Mg}/\text{Fe}]$.

The slopes of the $[\text{X}/\text{Fe}]$ -age relations (see Table 3) provide new information on the relative contribution of high- and low-mass supernovae to the nucleosynthesis of elements. Whereas the slope is positive or near zero for most elements, the *s*-process element yttrium stands out by having a strong negative abundance correlation with age. Over the lifetime of the Galactic disk, $[\text{Y}/\text{Mg}]$ increases by about 0.3 dex, which is probably due to an increasing contribution of yttrium from low-mass AGB stars relative to the contribution of magnesium from Type II SNe. This has led to the suggestion that $[\text{Y}/\text{Mg}]$ may be used as a sensitive clock to find ages of stars (Tucci Maia et al. 2016; Nissen 2016). It should, however, be noted that the tight $[\text{Y}/\text{Mg}]$ -age relation found in these papers and in the present work refers to stars with metallicities close to solar. Feltzing et al. (2017) have shown that the $[\text{Y}/\text{Mg}]$ -age relation depends on metallicity, so a $[\text{Fe}/\text{H}]$ term is needed for a proper calibration. Furthermore, the stars used to discover the $[\text{Y}/\text{Mg}]$ -age relation belong to the solar neighbourhood. A recent determination of $[\text{Y}/\text{Mg}]$ in K giants in four solar metallicity clusters with ages from 1 to 6 Gyr and distances up to 3 kpc by Slumstrup et al. (2017) suggests that the $[\text{Y}/\text{Mg}]$ -age relation is also valid outside the solar neighbourhood, but this should be verified for a larger sample of distant stars.

While the scatter in the $[\text{X}/\text{Fe}]$ -age relations are small for most elements, the scatter in $[\text{C}/\text{Fe}]$ and $[\text{O}/\text{Fe}]$ cannot be explained by observational errors in abundances and ages. Thus, we found two stars (KIC 6106415 and KIC 12258514) with about the same age and metallicity as the Sun, but with a difference $\Delta[\text{C}/\text{Fe}] = 0.092 \pm 0.028$ and a similar but less significant difference in $[\text{O}/\text{Fe}]$. Furthermore, the two stars have different slopes of $[\text{X}/\text{H}]$ versus elemental condensation temperature T_c (see Fig. 4). We also found the two components in the binary star 16 Cyg to have a small but significant difference in their $[\text{X}/\text{H}]$ - T_c slopes. These results point to variations in the volatile-to-refractory ratio in addition to changes caused by chemical evolution, for example due to planet-star interactions. This is a complication in Galactic archaeology when using abundance ratios for associating stars with a certain star-forming region (chemical tagging, Freeman & Bland-Hawthorn 2002). Abundance ratios of elements with similar condensation temperatures, such as Mg/Fe and Y/Al , seem better suited for chemical tagging than abundance ratios between elements with widely different values of T_c , such as C/Fe and O/Fe , but further studies of this problem are needed.

Acknowledgements. We thank Marcelo Tucci Maia for a constructive referee report and Anish Amarsi for helpful comments on the discussion of non-LTE and 3D effects. Based on observations made with the Italian Telescopio Nazionale Galileo (TNG) operated on the Island of La Palma by the Fundación Galileo Galilei of the INAF (Istituto Nazionale di Astrofisica) at the Spanish Observatorio del Roque de los Muchachos of the Instituto de Astrofísica Canarias. Funding for the Stellar Astrophysics Centre is provided by The Danish National Research Foundation (Grant agreement no.: DNRF106). This work has made use of data from the European Space Agency (ESA) mission *Gaia* (<https://www.cosmos.esa.int/gaia>), processed by the *Gaia* Data Processing and Analysis Consortium (DPAC, <https://www.cosmos.esa.int/web/gaia/dpac/consortium>). Funding for the DPAC has been provided by national institutions, in particular the institutions participating in the *Gaia* Multilateral Agreement.

References

- Adibekyan, V., Delgado-Mena, E., Feltzing, S., et al. 2017, *Astronomische Nachrichten*, 338, 442
- Adibekyan, V., Delgado-Mena, E., Figueira, P., et al. 2016, *A&A*, 592, A87
- Allende Prieto, C., Lambert, D. L., & Asplund, M. 2001, *ApJ*, 556, L63
- Amarsi, A. M. & Asplund, M. 2017, *MNRAS*, 464, 264
- Amarsi, A. M., Asplund, M., Collet, R., & Leenaarts, J. 2016a, *MNRAS*, 455, 3735
- Amarsi, A. M., Lind, K., Asplund, M., Barklem, P. S., & Collet, R. 2016b, *MNRAS*, 463, 1518
- Barklem, P. S., Belyaev, A. K., Spielfiedel, A., Guitou, M., & Feautrier, N. 2012, *A&A*, 541, A80
- Basu, S. & Antia, H. M. 2004, *ApJ*, 606, L85
- Bedell, M., Meléndez, J., Bean, J. L., et al. 2014, *ApJ*, 795, 23
- Belyaev, A. K. 2013, *A&A*, 560, A60
- Belyaev, A. K., Yakovleva, S. A., & Barklem, P. S. 2014, *A&A*, 572, A103
- Bergemann, M. 2011, *MNRAS*, 413, 2184
- Bergemann, M. & Cescutti, G. 2010, *A&A*, 522, A9
- Bergemann, M., Collet, R., Amarsi, A. M., et al. 2017, *ApJ*, 847, 15
- Bergemann, M., Kudritzki, R.-P., Gazak, Z., Davies, B., & Plez, B. 2015, *ApJ*, 804, 113
- Bergemann, M., Kudritzki, R.-P., Würl, M., et al. 2013, *ApJ*, 764, 115
- Bergemann, M. & Nordlander, T. 2014, *NLTE Radiative Transfer in Cool Stars*, ed. E. Niemczura, B. Smalley, & W. Pych, 169–185
- Bertran de Lis, S., Delgado Mena, E., Adibekyan, V. Z., Santos, N. C., & Sousa, S. G. 2015, *A&A*, 576, A89
- Böhm-Vitense, E. 1979, *ApJ*, 234, 521
- Bruntt, H., Basu, S., Smalley, B., et al. 2012, *MNRAS*, 423, 122
- Buchhave, L. A. & Latham, D. W. 2015, *ApJ*, 808, 187
- Carlos, M., Nissen, P. E., & Meléndez, J. 2016, *A&A*, 587, A100
- Christensen-Dalsgaard, J. 1988, in *IAU Symposium*, Vol. 123, *Advances in Helio- and Asteroseismology*, ed. J. Christensen-Dalsgaard & S. Frandsen, 295
- Christensen-Dalsgaard, J. 2008a, *Ap&SS*, 316, 113
- Christensen-Dalsgaard, J. 2008b, *Ap&SS*, 316, 13
- Christensen-Dalsgaard, J. 2016, *ArXiv e-prints* [arXiv:1602.06838]
- Christensen-Dalsgaard, J. & Pérez Hernández, F. 1991, in *Lecture Notes in Physics*, Berlin Springer Verlag, Vol. 388, *Challenges to Theories of the Structure of Moderate-Mass Stars*, ed. D. Gough & J. Toomre, 43
- Cochran, W. D., Hatzes, A. P., Butler, R. P., & Marcy, G. W. 1997, *ApJ*, 483, 457
- Cosentino, R., Lovis, C., Pepe, F., et al. 2012, in *Proc. SPIE*, Vol. 8446, *Ground-based and Airborne Instrumentation for Astronomy IV*, 84461V
- Davies, G. R., Chaplin, W. J., Farr, W. M., et al. 2015, *MNRAS*, 446, 2959
- Deal, M., Richard, O., & Vauclair, S. 2015, *A&A*, 584, A105
- D’Orazi, V., Magrini, L., Randich, S., et al. 2009, *ApJ*, 693, L31
- Dotter, A., Conroy, C., Cargile, P., & Asplund, M. 2017, *ApJ*, 840, 99
- Drawin, H. W. 1969, *Zeitschrift für Physik*, 225, 483
- Edvardsson, B., Andersen, J., Gustafsson, B., et al. 1993, *A&A*, 275, 101
- Feltzing, S., Howes, L. M., McMillan, P. J., & Stonkutė, E. 2017, *MNRAS*, 465, L109
- Flores, M., González, J. F., Jaque Arancibia, M., Buccino, A., & Saffe, C. 2016, *A&A*, 589, A135
- Freeman, K. & Bland-Hawthorn, J. 2002, *ARA&A*, 40, 487
- Gaia Collaboration, Prusti, T., de Bruijne, J. H. J., et al. 2016a, *A&A*, 595, A1
- Gaia Collaboration, Prusti, T., de Bruijne, J. H. J., et al. 2016b, *A&A*, 595, A1
- Gaidos, E. 2015, *ApJ*, 804, 40
- Gustafsson, B., Edvardsson, B., Eriksson, K., et al. 2008, *A&A*, 486, 951
- Hannaford, P., Lowe, R. M., Grevesse, N., Biemont, E., & Whaling, W. 1982, *ApJ*, 261, 736
- Haywood, M., Di Matteo, P., Snaith, O., & Lehnert, M. D. 2015, *A&A*, 579, A5
- Karakas, A. I. & Lugaro, M. 2016, *ApJ*, 825, 26
- King, J. R., Deliyannis, C. P., Hiltgen, D. D., et al. 1997, *AJ*, 113, 1871
- Kiselman, D. 1993, *A&A*, 275
- Kobayashi, C., Umeda, H., Nomoto, K., Tominaga, N., & Ohkubo, T. 2006, *ApJ*, 653, 1145
- Lambert, D. L. 1993, *Physica Scripta Volume T*, 47, 186
- Laws, C. & Gonzalez, G. 2001, *ApJ*, 553, 405
- Lind, K., Amarsi, A. M., Asplund, M., et al. 2017, *MNRAS*, 468, 4311
- Lind, K., Asplund, M., Barklem, P. S., & Belyaev, A. K. 2011, *A&A*, 528, A103
- Lind, K., Bergemann, M., & Asplund, M. 2012, *MNRAS*, 427, 50
- Lodders, K. 2003, *ApJ*, 591, 1220
- Lodders, K., Palme, H., & Gail, H.-P. 2009, *Landolt Börnstein* [arXiv:0901.1149]
- Lund, M. N., Silva Aguirre, V., Davies, G. R., et al. 2017, *ApJ*, 835, 172
- Magic, Z., Collet, R., Asplund, M., et al. 2013, *A&A*, 557, A26
- Mashonkina, L., Sitnova, T., & Belyaev, A. K. 2017, *A&A*, 605, A53
- Mashonkina, L. I., Belyaev, A. K., & Shi, J.-R. 2016, *Astronomy Letters*, 42, 366
- Meléndez, J., Asplund, M., Gustafsson, B., & Yong, D. 2009, *ApJ*, 704, L66

- Melendez, J. & Ramirez, I. 2016, ArXiv e-prints [arXiv:1611.04064]
Metcalf, T. S., Creevey, O. L., & Davies, G. R. 2015, ApJ, 811, L37
Minchev, I., Chiappini, C., & Martig, M. 2013, A&A, 558, A9
Minchev, I., Chiappini, C., & Martig, M. 2014, A&A, 572, A92
Nissen, P. E. 2015, A&A, 579, A52 (Paper I)
Nissen, P. E. 2016, A&A, 593, A65
Nordlander, T. & Lind, K. 2017, ArXiv e-prints [arXiv:1708.01949]
Önehag, A., Gustafsson, B., & Korn, A. 2014, A&A, 562, A102
Osorio, Y. & Barklem, P. S. 2016, A&A, 586, A120
Osorio, Y., Barklem, P. S., Lind, K., et al. 2015, A&A, 579, A53
Perets, H. B., Gal-Yam, A., Mazzali, P. A., et al. 2010, Nature, 465, 322
Press, W. H., Teukolsky, S. A., Vetterling, W. T., & Flannery, B. P. 1992, Numerical recipes in FORTRAN. The art of scientific computing (Cambridge: University Press, |c1992, 2nd ed.)
Ramírez, I., Meléndez, J., & Asplund, M. 2009, A&A, 508, L17
Ramírez, I., Meléndez, J., Cornejo, D., Roederer, I. U., & Fish, J. R. 2011, ApJ, 740, 76
Reddy, A. B. S. & Lambert, D. L. 2017, ApJ, 845, 151
Saffe, C., Jofré, E., Martioli, E., et al. 2017, A&A, 604, L4
Schuler, S. C., Cunha, K., Smith, V. V., et al. 2011, ApJ, 737, L32
Scott, P., Asplund, M., Grevesse, N., Bergemann, M., & Sauval, A. J. 2015, A&A, 573, A26
Silva Aguirre, V., Davies, G. R., Basu, S., et al. 2015, MNRAS, 452, 2127
Silva Aguirre, V., Lund, M. N., Antia, H. M., et al. 2017, ApJ, 835, 173
Slumstrup, D., Grundahl, F., Brogaard, K., et al. 2017, A&A, 604, L8
Spina, L., Meléndez, J., Karakas, A. I., et al. 2016a, A&A, 593, A125
Spina, L., Meléndez, J., & Ramírez, I. 2016b, A&A, 585, A152
Steenbock, W. & Holweger, H. 1984, A&A, 130, 319
Strömberg, B., Gustafsson, B., & Olsen, E. H. 1982, PASP, 94, 5
Takeda, Y., Hashimoto, O., Taguchi, H., et al. 2005, PASJ, 57, 751
Takeda, Y. & Honda, S. 2005, PASJ, 57, 65
Teske, J. K., Khanal, S., & Ramírez, I. 2016a, ApJ, 819, 19
Teske, J. K., Shectman, S. A., Vogt, S. S., et al. 2016b, AJ, 152, 167
Travaglio, C., Gallino, R., Arnone, E., et al. 2004, ApJ, 601, 864
Tucci Maia, M., Meléndez, J., & Ramírez, I. 2014, ApJ, 790, L25
Tucci Maia, M., Meléndez, J., Spina, L., & Lorenzo-Oliveira, D. 2017, MNRAS, submitted
Tucci Maia, M., Ramírez, I., Meléndez, J., et al. 2016, A&A, 590, A32
van Leeuwen, F. 2007, A&A, 474, 653
van Regemorter, H. 1962, ApJ, 136, 906
Verma, K., Faria, J. P., Antia, H. M., et al. 2014, ApJ, 790, 138
Vorontsov, S. V., Baturin, V. A., & Pamiatnykh, A. A. 1991, Nature, 349, 49
White, T. R., Huber, D., Maestro, V., et al. 2013, MNRAS, 433, 1262